

Unique strain history during ejection in canine left ventricle

A. S. DOUGLAS, E. K. RODRIGUEZ, W. O'DELL, AND W. C. HUNTER

Department of Biomedical Engineering, School of Medicine and Department of Mechanical Engineering, G.W.C. Whiting School of Engineering, The Johns Hopkins University, Baltimore, Maryland 21218

DOUGLAS, A. S., E. K. RODRIGUEZ, W. O'DELL, AND W. C. HUNTER. *Unique strain history during ejection in canine left ventricle*. *Am. J. Physiol.* 260 (Heart Circ. Physiol. 29): H1596–H1611, 1991.—Understanding the relationship between structure and function in the heart requires a knowledge of the connection between the local behavior of the myocardium (e.g., shortening) and the pumping action of the left ventricle. We asked the question, how do changes in preload and afterload affect the relationship between local myocardial deformation and ventricular volume? To study this, a set of small radiopaque beads was implanted in ~ 1 cm³ of the isolated canine heart left ventricular free wall. Using biplane cineradiography, we tracked the motion of these markers through various cardiac cycles (controlling pre- and afterload) using the relative motion of six markers to quantify the local three dimensional Lagrangian strain. Two different reference states (used to define the strains) were considered. First, we used the configuration of the heart at end diastole for that particular cardiac cycle to define the individual strains (which gave the local “shortening fraction”) and the ejection fraction. Second, we used a single reference state for all cardiac cycles i.e., the end-diastolic state at maximum volume, to define absolute strains (which gave local fractional length) and the volume fraction. The individual strain versus ejection fraction trajectories were dependent on preload and afterload. For any one heart, however, each component of absolute strain was more tightly correlated to volume fraction. Around each linear regression, the individual measurements of absolute strain scattered with standard errors that averaged $<7\%$ of their range. Thus the canine hearts examined had a preferred kinematic (shape) history during ejection, different from the kinematics of filling and independent of pre- or afterload and of stroke volume.

cardiac motion; cardiac kinematics; cardiac mechanics; ventricular volume; myocardial strains

THE ANALYSIS of biological systems often requires that the connection between structure and function be understood. For the heart, this requires that we understand the connection between the local action of the myocardium and the global function of the heart as a pump. With regard to deformation, global pumping function is characterized simply by parameters such as end-diastolic volume (EDV), end-systolic volume (ESV), stroke volume (SV), and ejection fraction. Local behavior of the myocardium is determined by its complex structure (20) and by the action of the sarcomeres. The structure is characterized by layers of unidirectionally oriented myocardial layers which vary in their preferred direction

through the thickness of the wall from epicardium to endocardium. The local change in the mechanical structure can be characterized by a number of parameters from percentage shortening in the hoop, longitudinal and thickness directions, and the shortening in the fiber and cross-fiber directions to local measures of strain. All of these measures quantify local myocardial performance that is directly related to the action of the sarcomeres (E. K. Rodriguez, W. C. Hunter, M. J. Royce, M. K. Leppo, A. S. Douglas, and H. K. Weisman, unpublished data).

It is the intent of this work to establish a connection between a local measure of myocardial tissue deformation (strain) and the global function (ejection or volume). Although three-dimensional strains have recently been measured in the left ventricle (27), no connection between the local strain and the global volume during the cardiac cycle has yet been drawn. McCulloch et al. (13, 14) have linked local and global deformations by measuring the superficial (epicardial) strain as a function of passive ventricular pressure or volume in the isolated arrested canine heart. In early models of ventricular mechanics, a unique relationship between strain and volume was assumed, but this cannot be universally true because it is known that strain is not constant under isovolumic contractions. For example, Olsen et al. (17) have shown that left ventricular eccentricity (a global measure) was a different linear function of ventricular volume during filling vs. ejection.

We examined whether the instantaneous sarcomere function, as characterized by the local deformation of the myocardium as ejection proceeds, was more closely related to the progressive amount of ejection defined by that particular cardiac cycle or to the instantaneous volume remaining in the ventricle. If, in the latter case, there was a relationship between local strain and volume strain independent of preload and afterload, then this would imply a direct coupling during ejection between sarcomere action and ventricular volume. Moreover, this relationship would indicate that there is some preferred sarcomere length and ventricular shape dependent primarily on the instantaneous volume during ejection for a given contractile state. To establish such a relationship it was necessary to define a strain (which is a relative measure of change in length) with respect to an appropriate single reference length and a normalized measure of the volume remaining. Since the three-dimensional

Lagrangian strain at a point completely described the local mechanical action of the sarcomeres, this strain was related to a normalized measure of the instantaneous volume remaining in the ventricle called the volume strain.

We thus measured the instantaneous local myocardial position of six markers in the left ventricular wall. This motion was quantified by the Lagrangian strain relative to both a single (absolute) reference state for each heart and an individual reference state defined at end-diastole for that particular cardiac cycle. Simultaneously, the instantaneous chamber volume was recorded. Through the use of physiologically realistic pressure and volume cycles, the afterload and preload could be varied widely in the isolated canine heart.

We found that throughout much of ejection, there was a strong coupling between the components of strain and the volume strain when referenced to a single common (or absolute) reference state for each heart. In contrast, the strain relative to an individual reference for each cycle, when examined as a function of instantaneous ejection fraction for that cycle, depended on the specific hemodynamic conditions governing that particular cardiac cycle.

METHODS

Overview: A quantitative description of the deformation of a body can be obtained by comparing the spatial positions of internal points at any two different states. By sampling the relative motion of only a limited number of points, an approximate description of the local deformation can be determined (2, 10). In this study of local cardiac deformation, radiopaque markers were implanted in a region of the free wall of the left ventricle of live canine hearts, and the bead positions were then recorded using biplane cineradiography while they moved within the beating heart (5), from which a quantitative description of deformation could be obtained. This technique has been used previously by several laboratories studying regional cardiac deformation (3, 15, 27). The main advantage of having beads set in the heart is that their relative motion accurately reflects the deformation of a well-defined region of the neighboring myocardium during an experiment. The errors inherent in such a procedure, which have been quantified (2), are small enough to allow an adequate description of local myocardial deformation to be obtained.

Marker implantation. The motion of four points that form a tetrahedron in a region is the minimum required to define the deformation or strain in that region (2, 27). However, since greater accuracy in determining the homogeneous deformation is obtained using six markers that form a prism (2), we implanted nine radiopaque markers in the ventricular myocardium, defining two six-bead prisms. The markers were 1 mm diameter stainless steel beads (i.e., ball-bearings, Winstead Precision, Winstead, CT). Figure 1 shows how, in each of the three layers, these beads were placed approximately at the apexes of an equilateral triangle 1 cm on a side, and in each layer corresponding beads were placed at approxi-

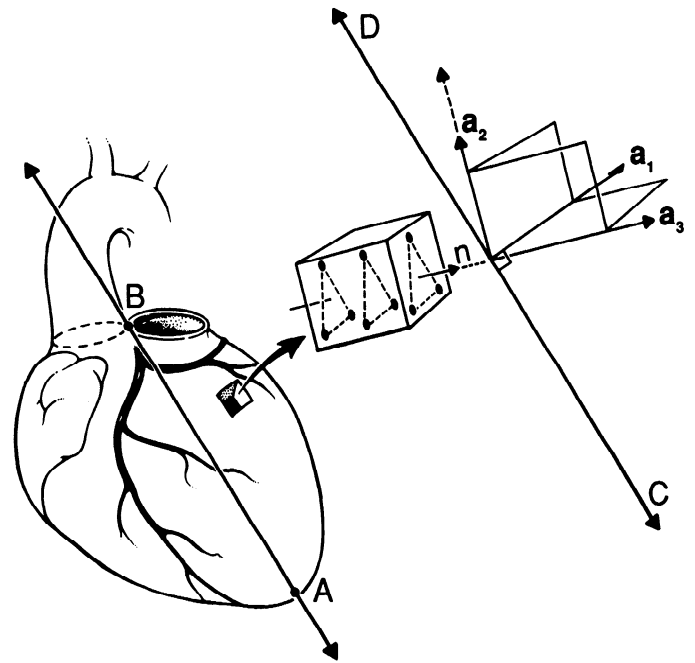


FIG. 1. Schematic view of a heart in one of its reference states showing definition of local coordinate system. Note the 9 implanted beads (a triangle in each of 3 parallel layers), apical bead A, and basal bead B. Axis CD is parallel to AB and passes through the centroid of the 3 epicardial beads. The normal to these 3 beads (n) represents the local radial direction vector (a_3). The local circumferential unit vector (a_1) is perpendicular to both a_3 and to CD. Unit vector a_2 is perpendicular to both these 2 unit vectors and represents the local meridional direction.

mately the same position relative to the axis and equator of the left ventricle. The layers were ~3–4 mm apart.

The implanted region was located in the lateral free wall of the left ventricle near the equator (i.e., the region of largest transverse diameter, which was $\sim\frac{1}{4}$ to $\frac{1}{3}$ of the distance from base to apex), as shown in Fig. 1. In this vicinity, we sought a zone that was free of large epicardial coronary vessels, and we also oriented the implantation triangle to avoid vessels.

Bead implantation was performed under sterile surgical conditions in mongrel dogs weighing 18–22 kg. After overnight fasting, the dog was anesthetized with pentobarbital sodium (30 mg/kg). The heart was exposed via a left thoracotomy at the fifth intercostal space. The pericardium was incised parallel to the left ventricular axis. The visceral pericardial membrane, which sheaths the epicardial myocardium, was punctured at three points that defined the triangular implantation pattern. Each bead to be implanted was held by suction at the tip of a specially machined needle (19). After inserting the needle perpendicularly into the myocardium to the desired depth, implantation was completed by breaking suction (often with a small burst of positive pressure) and slowly withdrawing the needle. An initial triplet of beads was implanted at 8 mm depth; using the same needle pathways, a second triplet was then implanted at 4 mm depth. Finally, three beads forming an epicardial layer were implanted individually by sliding a needle underneath the visceral pericardial membrane tangential to the epicardium for a few millimeters away from the

site of each needle puncture. Following implantation, the pericardium was reapproximated before closing the chest.

Isolated heart preparation. After 7–10 days were allowed for the heart to recover from implantation and for the beads to become more firmly imbedded in the myocardium (19), the dog was anesthetized (pentobarbital sodium, 40 mg/kg). Its heart was isolated from the systemic and pulmonary vasculature, supported by cross-circulation from a support dog, and excised (21). This isolated heart preparation allowed us to measure left ventricular cavity volume while controlling the load during each stage of the cardiac cycle (including active systolic ejection by the isolated heart). Thus we could compare ventricular cavity volume, a measure of global distension, to the estimate of local deformation. In contrast to the *in situ* heart, however, coronary perfusion pressure was maintained constant despite changes in systolic pressure generated by the left ventricle.

Details of the isolated heart preparation have been reported previously (21). Briefly, after the chordae tendinae was cut and a support ring was sutured to the mitral annulus, a water-filled latex balloon was inserted into the left ventricular chamber. This balloon was connected to a servo pump that controlled ventricular volume. The volume servo system was itself controlled by a computer simulation of the vascular afterload that limited the amount and nature of active ejection, so that the cardiac cycle followed physiologically shaped pressure-volume loops (23). By varying the simulated filling pressure and afterload resistance, both end-diastolic volume and stroke volume could be varied over a wide range. Contractility, while not explicitly varied in these experiments, might vary spontaneously during any experiment.

The cineradiographic equipment required the heart to be situated with its axis held horizontally instead of vertically. To support the heart in this orientation, an artificial "pericardial" cradle (composed of a thin sheet of flexible plastic) was placed underneath and around the sides of the isolated heart. The height of this cradle was adjusted so that the left ventricular axis was approximately horizontal and orthogonal to the ring sutured into the mitral plane. To identify the left ventricular axis radiographically, two additional markers were sutured to the heart; one was placed near the apical dimple and the other was sutured to the fibrous ring at the root of the aorta between mitral and aortic valves.

*Recording and calculation of *in vivo* marker motion.* The isolated heart with implanted beads was then imaged in a General Electric biplane cineradiography system (model MS1-850-II) set to 6-in. imaging mode (5) at 80 kVA. Images from both the lateral and vertical X rays were simultaneously recorded on two Cinerex PFA catheterization films at 90 frames/s.

To translate the images recorded on biplane films into the spatial coordinates of each bead, we used a special purpose digital image processing system (5, 10). Briefly, one frame from a cine film was projected (using Vanguard Instrument model M-35C) into the optics of a video camera (Panasonic model WV-BL200). The video image was digitized at a resolution of 512×480 pixels. A

computer tracking algorithm then found the center of each bead image by matching the observed intensity profile with various x - y displacements of the expected intensity profile. This method of comparing the two-dimensional distribution of image intensities in the neighborhood of each real bead image with an ideal image gives the position of the bead to within a root-mean-square accuracy of 0.1 mm (5). After this procedure was repeated for the orthogonal view, the planar coordinates from both views were combined to determine the three-dimensional location of each bead. This process was repeated for each frame. One to three cardiac cycles were spanned for each data set.

Determination of strain. During these experiments the active isolated heart deformed to fill and eject blood with each cardiac cycle, resulting in an *inhomogeneous* motion of the cardiac muscle. The bulk motion of any small region of the heart was made up of both a rigid-body motion, which included translation and rotation, and a deformation. The deformation gave rise to a stretching or contraction of the tissue in any direction that could be quantified by determining the Lagrangian strain (12) for that small region. Throughout the whole heart, the deformations, and hence the strain, varied. Since myocardium is nearly incompressible, the deformation varied with position through the heart wall (2).

Even though the cardiac deformation was inhomogeneous, in any small enough region, the deformation could be characterized approximately by a uniform stretch in three orthogonal directions followed by a rigid-body rotation (2). This combined motion, which related the relative position of any two sufficiently close neighboring points in the deformed position to their relative position in a reference state, was quantified by the deformation gradient tensor \mathbf{F} (12). It should be noted that in the absence of a clearly defined stress-free configuration, there is no unique way to choose a reference state.

Two different reference states were used here to compute the deformation gradient tensor \mathbf{F} and hence the strains. The first was the cardiac configuration at end diastole for each individual cardiac cycle under consideration. [This is the method used in all previous computations of systolic local myocardial strain (3, 15, 25, 27).] The second was to use a single reference state for any one heart, chosen to be the end-diastolic state having maximum volume for all cycles. This (absolute) reference state is close to the maximum volume configuration, which was defined as the EDV when the end-diastolic pressure (EDP) was 16–21 mmHg. Hittinger et al. (7) also used both a single fixed reference length and the end-diastolic length of that beat to compute the one-dimensional myocardial stretch observed using a pair of ultrasonic crystals.

The Lagrangian strain tensor \mathbf{E} was used to quantify that component of the motion that results only from deformation, explicitly excluding rigid-body translation and rotation, and is defined (12) by

$$\mathbf{E}(t) = [\mathbf{F}^T(t) \cdot \mathbf{F}(t) - \mathbf{I}]/2 \quad (1)$$

where \mathbf{I} is the identity tensor, \mathbf{F}^T is the transpose of \mathbf{F} ,

and both \mathbf{E} and \mathbf{F} are functions of time t . This is the same strain measure that was used by Waldman et al. (27). In any given direction, the Lagrangian strain, \mathbf{E} , gives one-half of the change in squared length per unit reference squared length at time t . For small deformations, this strain measure reduces to the infinitesimal strain tensor that gives the change in length per reference length (12).

Four non-coplanar markers defining a tetrahedron are the minimum number necessary to define the homogeneous state of strain in that region. Six markers defining a prism can give some higher-order information, but this additional information can also be used to minimize both the error in the location of the marker beads and the errors inherent in determining homogeneous strains from the motion of discrete points (2). To quantify the strains resulting from the deformation of the muscle fibers, the optimal (in a least-squares sense) homogeneous strain was used here. The motion of the region of ventricular wall spanned by the six marker beads was broken down into a local translation of the centroid and a uniform deformation gradient \mathbf{F} with respect to both the individual (the end-diastolic state for that cardiac cycle) and absolute (maximum end-diastolic volume over all cycles) reference states. If only five beads were available, the same procedures applied but resulted in less error reduction in the data used to compute \mathbf{F} . The strains were then computed using Eq. 1. A detailed description of the method used to compute the deformation gradient and the strain is given in APPENDIXES A and B.

The strains were represented by a matrix of six tensor components (since \mathbf{E} is a symmetric tensor) with respect to the cardiac coordinates shown in Fig. 1. In the chosen reference state, the apical bead A and basal bead B defined the longitudinal cardiac axis, while the normal to the three epicardial beads $\mathbf{n} = \mathbf{a}_3$ defined the radial unit vector. The circumferential unit vector \mathbf{a}_1 was defined to be normal to both the base-apex direction (AB or CD in Fig. 1) and \mathbf{a}_3 . The local meridional unit vector was defined as $\mathbf{a}_2 = \mathbf{a}_3 \times \mathbf{a}_1$ and completed the local orthonormal coordinate system (see Fig. 1).

RESULTS

Deformation measures. In the cardiac coordinate system defined above, the strain components E_{11} , E_{22} , E_{33} , corresponded to the extensional strains in the circumferential direction, the local meridional direction, and the radial direction, respectively. These directions are shown in Fig. 1. As shown in Fig. 3, where the arrows indicate the part of the myocardial strain vs. volume strain loop corresponding to ejection, the strains E_{11} and E_{22} decreased as the circumferential and base-apex dimensions of the heart reduced to lower the ventricular cavity volume, indicating a local myocardial shortening in circumferential and meridional directions. The radial strain E_{33} was directly related to the local wall thickening that, in any cardiac cycle, increased during ejection, as shown in Fig. 3.

The shear components E_{12} , E_{13} , and E_{23} quantify the

distortion of the heart. The circumferential-longitudinal shear strain is given by E_{12} , which represents a reorientation of the myofibers (28) caused by the local twisting of the heart around the base-apex axis. The shear E_{13} is caused primarily by a difference in rotation around the base-apex axis of the endocardium and the epicardium. The shear strain E_{23} is influenced by the difference in meridional shortening through the heart wall.

Two normalized measures of volume were considered. First, the volume strain was defined by the instantaneous ventricular volume V and the reference volume V_{\max} , as

$$\text{volume strain} = (V - V_{\max})/V_{\max}$$

where the reference volume V_{\max} was given by the maximum volume at end diastole when the EDP was 16–21 mmHg. The volume V_{\max} was the ventricular cavity volume in the same cardiac state used to define the absolute reference state for the strains. The volume strain is a normalized measure of the instantaneous volume remaining in the ventricle. Second, we defined the instantaneous ejection fraction by

$$\text{ejection fraction} = (V - \text{EDV})/\text{EDV}$$

which is consistent with the definition of volume fraction but results in the negative of the usual definition of ejection fraction. Note that for each heart, one cardiac cycle had $\text{EDV} = V_{\max}$, which means that for that one loop both measures of strain were equivalent and volume strain equaled ejection fraction.

Typical cardiac response. Heart 1 was subjected to the pressure-volume (P-V) histories shown in Fig. 2 and provided data representative of that obtained for all six hearts examined. Strain histories were obtained with each heart for a number of different cardiac cycles with different pre- and afterloads and with different end-systolic pressures. For example, in the four different P-V loops shown for heart 1 in Fig. 2, runs 1, 3, and 4 have

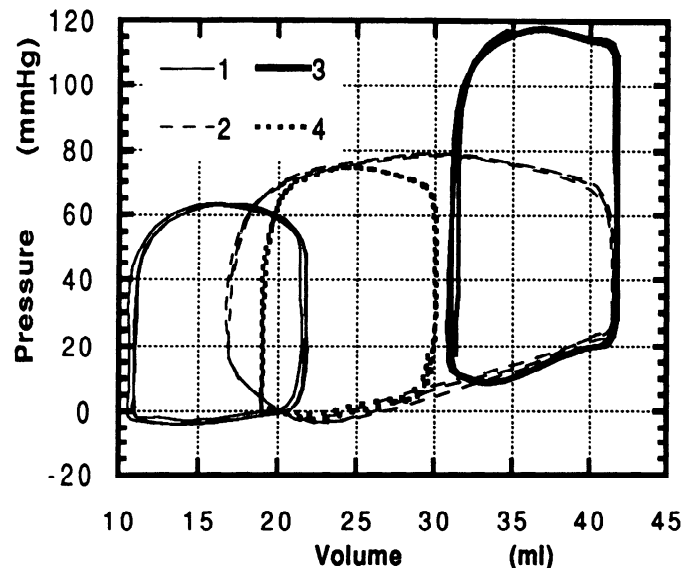


FIG. 2. Pressure vs. volume loops for heart 1 for loading conditions examined in Figs. 3–5. (Note that contractility may have varied slightly between loading conditions.)

similar stroke volumes but different absolute volumes. *Run 2* has a larger ejection fraction but the same EDV as *run 4*. Each has a different afterload.

The entire strain histories for each of the six independent strain components in the midwall are shown in Figs. 3 and 4. The strains in the subepicardial region are similar to the strains in the midwall, as can be seen by comparing Figs. 3 and 5, which show the three extensional strains. In each figure the left panels show the relationship between one strain component when defined with reference to the single (absolute) reference state and the volume strain. The right panels show strain components defined with reference to the EDV state for that individual P-V loop. Thus, in each right panel, the strain component is zero at zero ejection fraction (corresponding to the EDV). For *heart 1*, *run 3* had the maximum EDV. Therefore, for *run 3* only, $V_{\max} = \text{EDV}$, volume strain = ejection fraction, and absolute strains are identical to individual strains. This can be seen in Figs. 3–5, where the strain cycles for *run 3* are the same

in each left panel as they are in the corresponding right panel.

Figures 3 and 5 show the extensional strain histories. Three cardiac cycles form each of the four circumferential strain E_{11} vs. volume strain loops. End diastole is at the lower right corner of each loop (both left and right panels). This is followed by the isovolumic contraction, during which the circumferential strain E_{11} increased. This strain then decreased during ejection (along the arrows) and continued to decrease during isovolumic relaxation. During filling E_{11} increased, returning to the end-diastolic state. When viewed as absolute strain vs. volume strain, the relationship between E_{11} and volume strain during ejection was independent of cardiac cycle and fell along a straight line roughly parallel to the arrows drawn to indicate ejection. In the right panel, all the cardiac cycles have zero individual strain at the EDV, so all loops have a common starting point. However, the individual strain E_{11} vs. ejection fraction (shown in the right panel) displayed no clear relationship. This trend

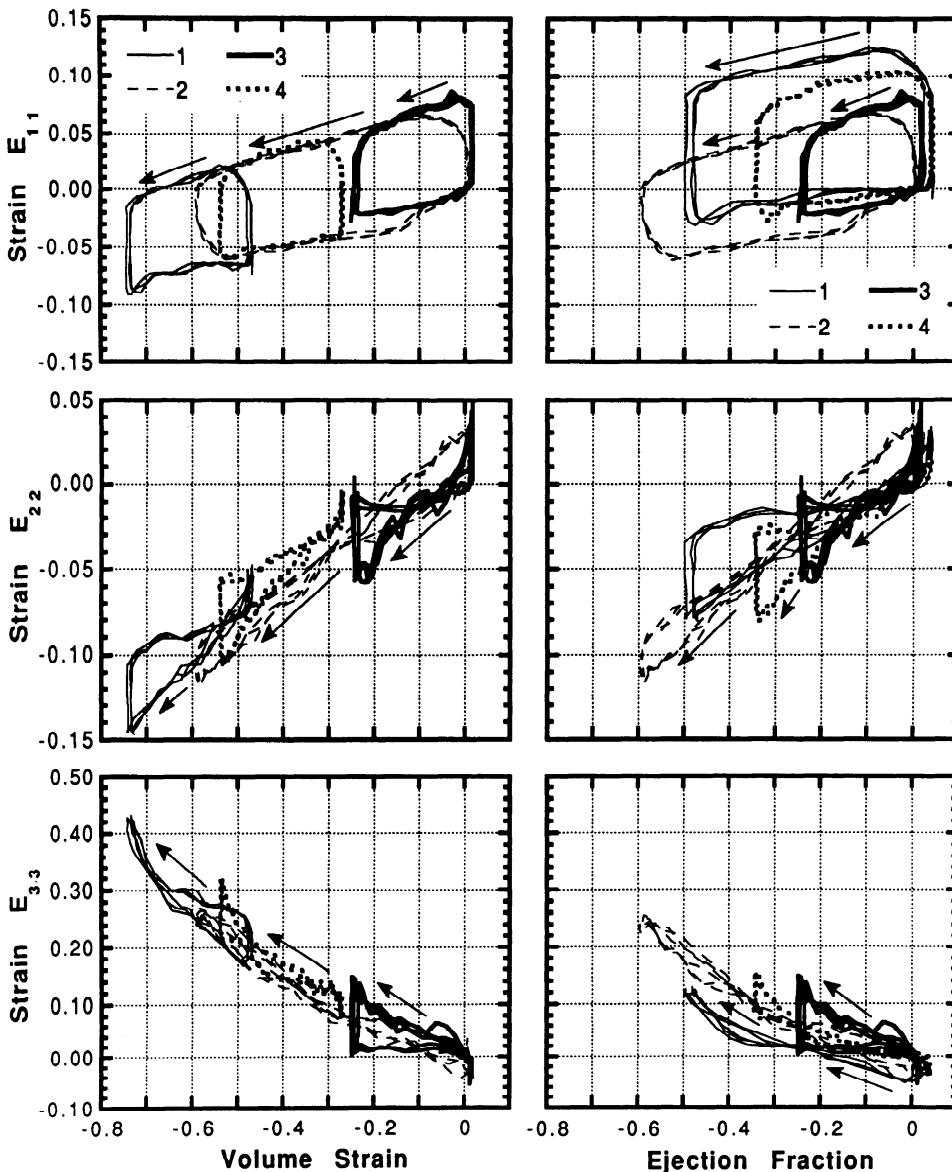


FIG. 3. Extensional strains (measured near the midwall of the myocardium) vs. volume strain or ejection fraction for *heart 1*. Left panels relate absolute strains (only 1 reference state) to volume strain. Right panels relate individual strains (a new reference state for each hemodynamic state) to ejection fraction. Arrows indicate ejection phase of cardiac cycle.

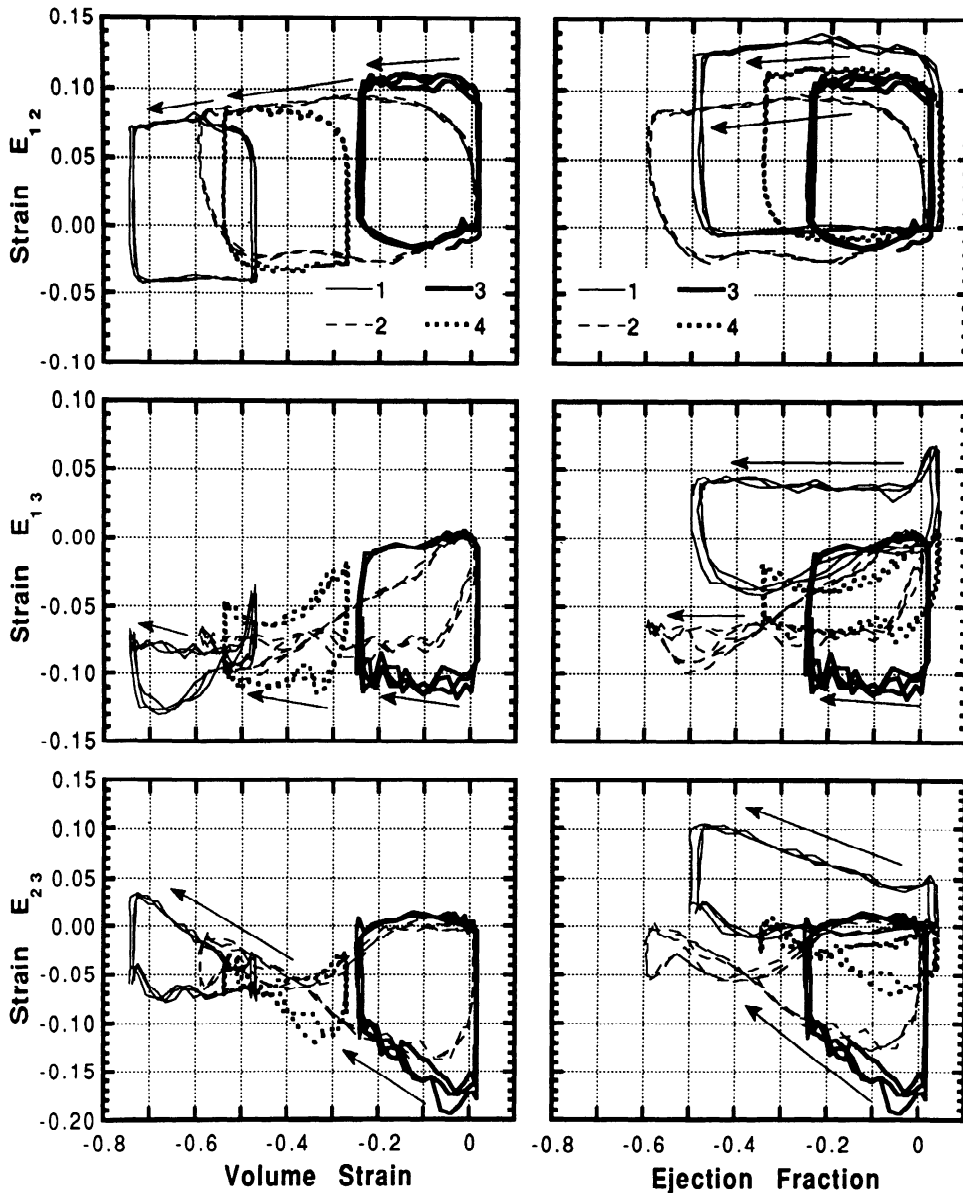


FIG. 4. Shear strains (near the mid-wall) vs. volume strain or ejection fraction for same cardiac cycles shown in Fig. 3 in *heart 1*. Left panels relate absolute strains (only 1 reference state) to volume strain. Right panels relate individual strains (a different reference state for each hemodynamic state) to ejection fraction. Arrows indicate ejection.

is made clearer by Figs. 6 and 7, which show the ejection phase only identifying the linear relationship between absolute strain E_{11} and volume strain.

The strain E_{22} also followed a pattern of decreasing with the contraction and increasing during filling, but the isovolumic changes in E_{22} were not as pronounced as for the strain E_{11} . Again there was direct relationship between volume strain and absolute extensional strain E_{22} . However, for the individual strain E_{22} vs. ejection fraction, there was also a consistent relationship independent of cardiac cycle. The local radial thickening as quantified by the strain E_{33} followed the expected pattern of increasing (thickening) with the contraction and decreasing during filling.

In Fig. 4 the shearing strain components are presented for the inner prism. The strain E_{12} has a behavior similar to the strain E_{11} , clearly indicating a large twisting and untwisting of the left ventricle during the two isovolumic phases. During ejection *heart 1* showed a clear linear relationship between absolute strain E_{12} and volume

strain. Even more remarkable is the strain E_{23} in Fig. 4. *Run 1* has a counterclockwise absolute strain vs. volume strain loop while *run 3* ran clockwise and *runs 2* and *4* traced lopsided bow ties. However, although the shape of the loop was different during ejection, the absolute strain E_{23} followed a linear relationship with volume strain. Relating individual strain to ejection fraction shows no common trend other than an increase in strain E_{23} with ejection.

Although the extensional strains near the midwall are larger than those in the subepicardial region, there is a strong similarity between these strains, as shown in Figs. 3 and 5. This is also true for the shear strains near the midwall (shown in Fig. 4) and those near the epicardium (not shown).

Ejection in a typical heart. The linear relationship between absolute strain and volume strain during ejection (here defined to be the central 80% of the stroke) is clarified by examining Figs. 6 and 7 (for the region of myocardium near the midwall), which show the ejection

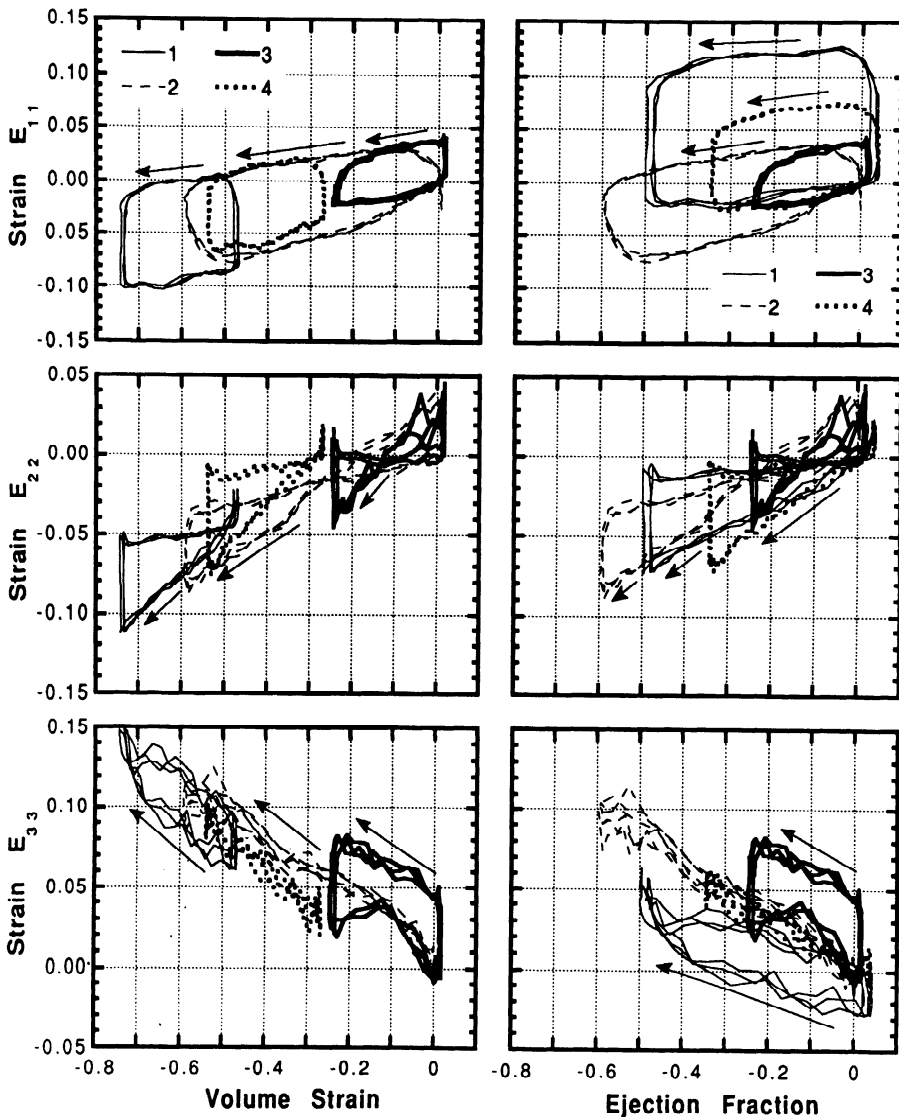


FIG. 5. Extensional strains vs. volume strain (left panels) or ejection fraction (right panels) for subepicardial region of *heart 1*. Left panels relate absolute strains to volume strain. Right panels relate individual strains to ejection fraction. Arrows indicate ejection phase of cardiac cycle. Note the similarity with strains shown in Fig. 3 for the midwall.

only data for *heart 1*. Again, while not shown, the data for the epicardial region are very similar to the midwall data.

In Fig. 6 the absolute strains E_{11} vs. volume strain fell along a single line for all of the four P-V loops shown in Fig. 2. Thus, regardless of afterload, preload and phase in the cycle, a single unique pathway related absolute strain E_{11} to volume strain throughout ejection in *heart 1*. No common pathway was found when the strain was computed using individual reference states and plotted as a function of ejection fraction. Indeed, three separate E_{11} strain pathways depending on the preload could be identified. In the right panel, runs 2 and 3 had the same pathway because their EDVs, and hence their reference states, were very close even though their degrees of ejection were very different.

This same pattern was also true for the strain components E_{33} , E_{12} , E_{13} , and E_{23} in Figs. 6 and 7 where the absolute strains vs. volume strain showed a common ejection pathway more clearly than the individual strain components vs. ejection fraction. In Fig. 6 the strain component E_{22} did not clearly define a single linear relationship but, in common with all the other strain

components, showed a clear trend in the four parallel pathways for each individual loop.

Comparing the left hand panels relating absolute strain to volume strain with the right panels relating individual strains to ejection fraction in Figs. 3–7, one important observation must be made. The absolute strain components (particularly E_{11} and E_{12} , but also E_{22} , E_{13} , and E_{23}) vs. volume strain showed a clear cycle-independent linear relationship during ejection. The same was not, in general, true for the individual strains vs. ejection fraction.

Comparison of six hearts. Having examined *heart 1* in some detail, it is imperative to see if the same results are found in a statistically significant sample of other canine left ventricles. Figures 8–10 show comparisons of the absolute and individual circumferential strain E_{11} and shearing strains E_{12} (which is indicative of the local twisting of the heart around the base-apex axis) and E_{23} respectively vs. volume strain and ejection fraction for six canine hearts. In Fig. 8 in each of the left panels, the absolute circumferential strains E_{11} vs. volume strain fell along a common linear trajectory. The right panels show the individual strains vs. ejection fraction, which in

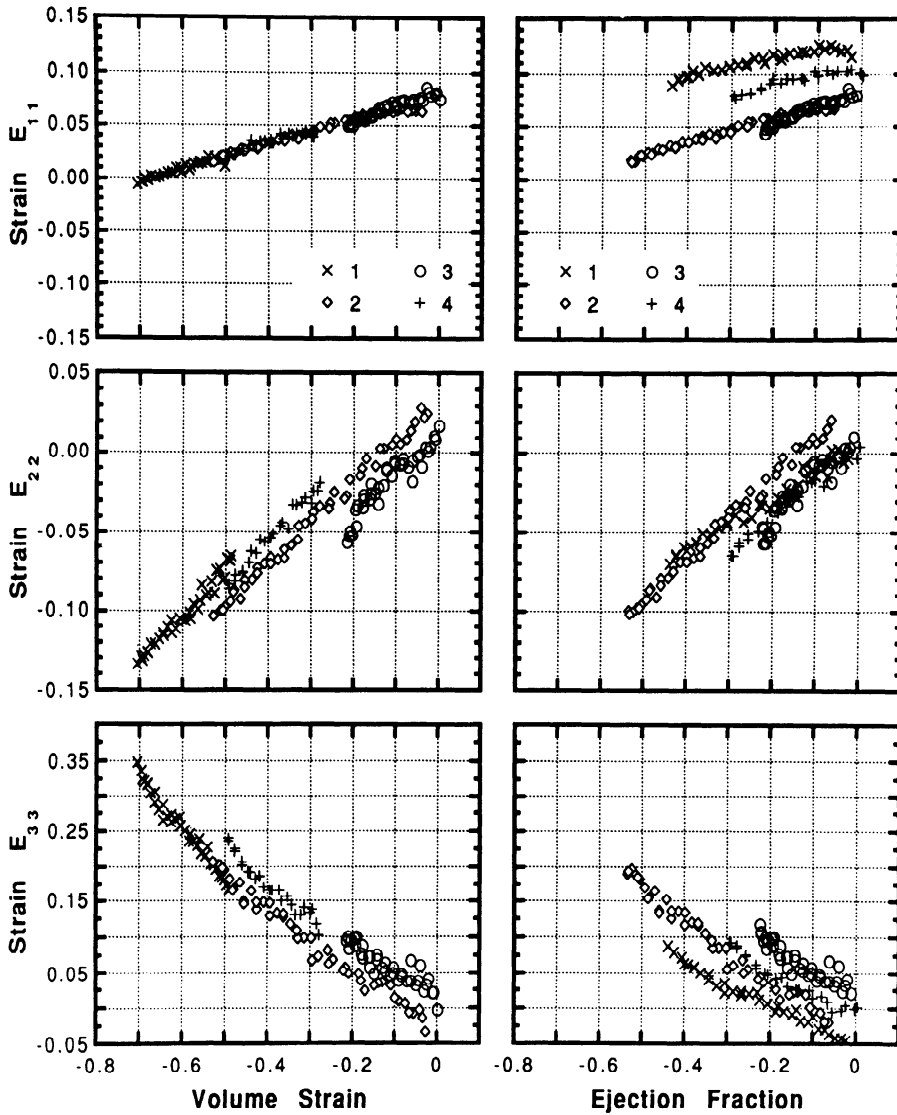


FIG. 6. Ejection phase only data excerpted from Fig. 3 showing extensional strains vs. volume strain or ejection fraction for heart 1 near the midwall. Note that absolute strains in left panels have a common linear relationship with volume strain.

general did not follow a single linear path as closely as the data in the left panels. *Heart 1* showed the greatest difference between individual strains vs. ejection fraction because the individual end-diastolic reference states were most different. Also, the isovolumic strain changes in *heart 1* were greater than in the other hearts. Only in *heart 5* could a common relationship among the individually referenced strains be thought to have held for each of the six hemodynamic loads examined in that heart. The use of a single reference for strain and a common volume measure (volume strain) allows us to identify a linear relationship between local deformation and global volume that is independent of the cardiac cycle. For example in *heart 6*, run 2 (squares) has a comparatively low EDV, so that in the right panel it appeared to be different from the other loading states. In the left panel, on the other hand, the absolute myocardial strain vs. volume strain was clearly on a line common to other absolute myocardial strain vs. volume strain paths generated by very different loading conditions.

The local base-apex twisting strain, E_{12} , shown in Fig. 9, also displayed a linear relationship (left panels) for each of *hearts 2* through *6* with tighter bounds than for

heart 1. In Fig. 10, the shearing strain E_{23} showed that *hearts 1, 2, 4, and 6* were clearly linear, while *hearts 3 and 5* did not exhibit as well-defined a common linear behavior. These strains were computed using radial information, which is not only subject to the most experimental error but also shows the greatest transmural variation (2). As the figures confirm, the shear strain components E_{12} and E_{23} followed the same pattern of behavior as the circumferential strain E_{11} : there was almost always a more direct relationship between the absolutely referenced strains and cavity volume than between the individually referenced strains and ejection fraction.

Quantitative analysis. We wished to quantify the extent to which a single linear relationship existed between the absolute strains and the volume strain and to compare that with any relationship between the measures for an individual beat, namely the individual strain vs. ejection fraction. To do this we used linear regression to fit a straight line through the ejection-phase data from all loading conditions for a single heart. The standard error of the estimate (SEE) was used to quantify the variance around this regression line (6). The SEE results are given

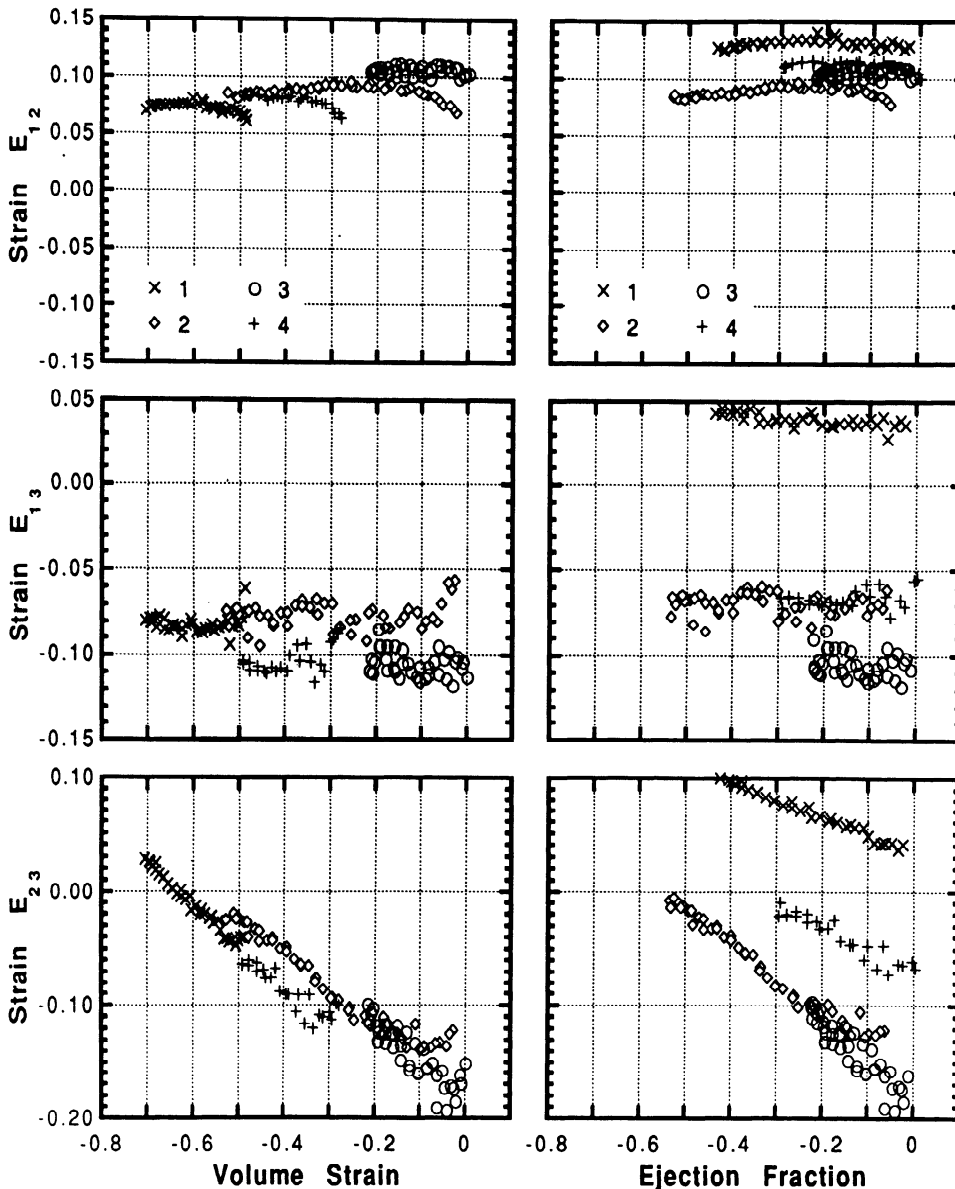


FIG. 7. Ejection phase only data excerpted from Fig. 4 showing shear strains vs. volume strain or ejection fraction for heart 1 near the midwall. Note that absolute strains in left panels have a common linear relationship with volume strain.

in terms of the dependent variable, i.e., the strains, and should be compared with typical strain values as shown in the figures, which range from -0.15 to $+0.15$. All the strain components had a maximum range (during an entire cardiac cycle) of $\sim 15\%$.

Figure 11 graphically depicts the comparison of the SEE for all six strain components in all six hearts for the epicardial myocardium, and it clearly shows two important results. First, in 33 of 36 cases the SEE of the absolute strains (A) was lower than the SEE of the individual strains (I). Second, for the absolute strains, the SEE was always small. For the strains E_{11} and E_{12} the SEE normalized by the total strain range averaged 4% with a maximum of 6%. When normalized by the strain range during ejection only the SEE for E_{11} and E_{12} was $<20\%$. The strains E_{22} and E_{13} had an average SEE of 6% of the total strain range, with a maximum $<13\%$. The SEE for the strain E_{23} was only slightly higher, with an average of 7% and a maximum of 14% of the total strain range. As expected, because radial strains have the

most experimental error, the maximum absolute value of the SEE for E_{33} in one heart was the largest (almost 0.04), but, as a percentage of the strain during ejection, this was $<27\%$. The SEE normalized by the total strain range for E_{33} averaged 16%, with a maximum of $<25\%$. The average of all the SEE for all strain components in all hearts normalized by their respective strain ranges was 7.1%.

A comparison between absolute and individual strains in the midwall region and the subepicardial region of heart 1 (Fig. 3 vs. Fig. 4) shows that there was little difference in the extent to which a linear relationship held at the two myocardial depths. This trend was confirmed by SEE analysis for the midwall section, for which results very similar to those mentioned above were obtained.

DISCUSSION

This study was the first work to examine the local three-dimensional strains in a lateral region of the ven-

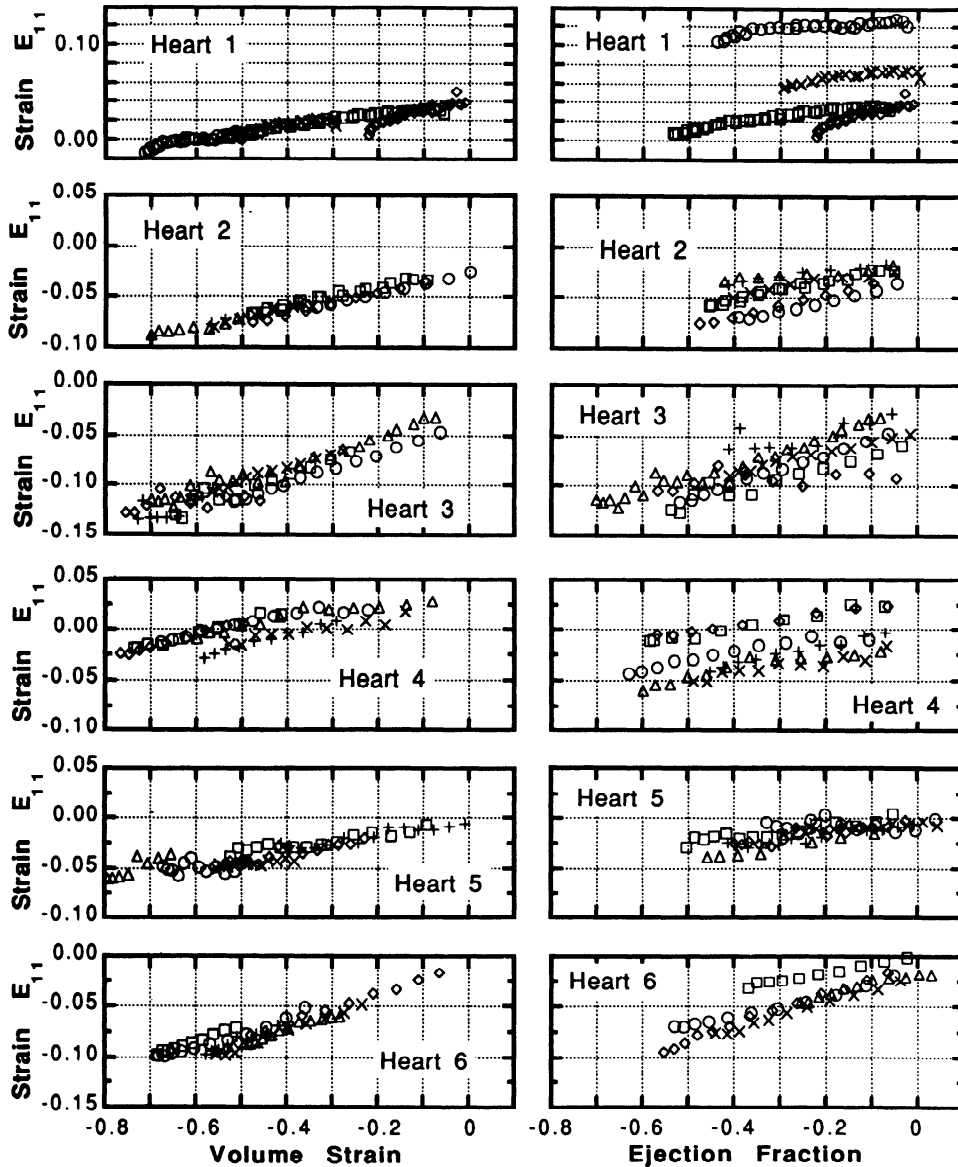


FIG. 8. Comparison among all 6 hearts of the circumferential strain as a function of volume strain and ejection fraction during ejection only. Each of the 6 data sets for any 1 heart refers to a different hemodynamic state having varied preload and afterload. Note that absolute strains in left panels have a common linear relationship with volume strain compared with the more varied relationships between individual strain and ejection fraction (right panels).

tricular free wall as a function of ventricular volume for different end-diastolic and stroke volumes. We asked the question, how do changes in preload and afterload affect the relationship between the local myocardial deformation in the free wall and the instantaneous ventricular volume? By referring strain to the configuration of the heart at end diastole for any given cardiac cycle, we defined the individual strains (which gave a measure of the local "shortening fraction"). The ejection fraction was also defined relative to end diastole for any cardiac cycle. Alternatively, for any one heart, we also used a single reference state for all cardiac cycles, the end-diastolic state at maximum volume, to define absolute strains (which gave local fractional length). The volume fraction was also defined with reference to this maximum-volume end-diastolic configuration. The volume fraction was therefore a direct measure of the volume remaining in the ventricle independent of the cardiac cycle. The individual strain vs. ejection fraction trajectories varied considerably, depending on preload and

afterload. For any one heart, however, each component of absolute strain was tightly correlated to volume fraction independent of afterload and preload. Around each linear regression, the individual measurements of absolute strain scattered with standard errors that averaged $\sim 7\%$ of their total strain range.

Significance of strain-volume relationship. Since the absolute strain vs. volume strain relationship is essentially independent of the preload and afterload, each heart must have a preferred kinematic configuration during ejection dependent primarily on instantaneous ventricular volume and relatively independent of the instantaneous ventricular pressure and the history of deformation (i.e., end-diastolic volume and the amount of ejection preceding that instantaneous volume).

Consider the strain components during ejection in *heart 1* shown in Figs. 6 and 7. As the pressure-volume loops show (Fig. 2), *cycles 2* and *3* ejected against different afterloads from the same preload. This means that, for a given volume strain, the pressure must be higher for *cycle*

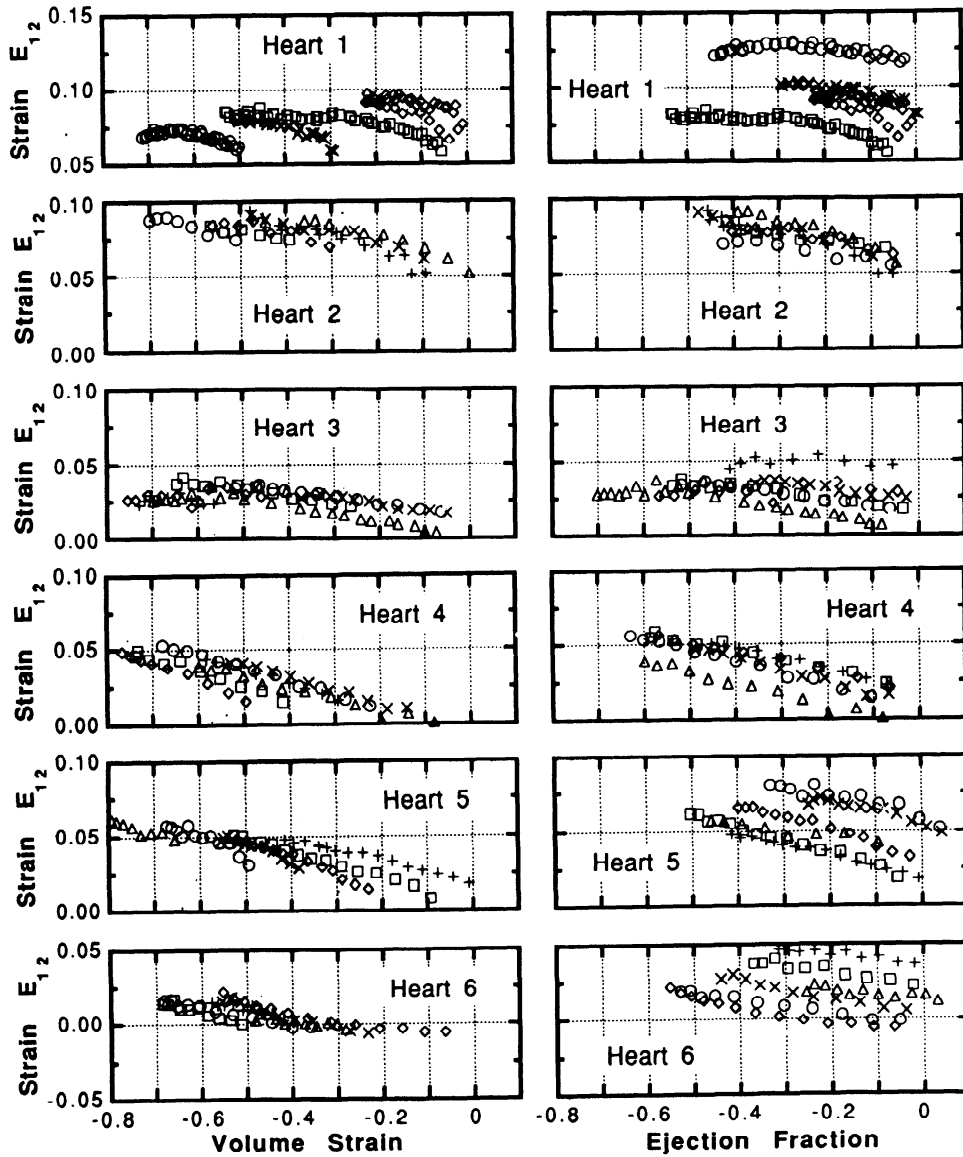


FIG. 9. Comparison among all 6 hearts of the shear strain E_{12} as a function of volume strain and ejection fraction during ejection only. These shear strains result from twisting of the heart around its base-apex axis.

3 than for cycle 2. Despite differences in pressure, the strain components for both these two cycles (and in fact, for any cycle) had essentially the same linear relationship with volume strain during ejection. Thus the deformation of the myocardial components (including the sarcomeres) was uniquely related to ventricular volume independent of stress level.

For ejections originating from different end-diastolic volumes, the same unique relationship between absolute strain and volume strain remained valid. As Fig. 2 shows, cycles 1, 2, and 4 ejected over very different stroke volumes and from different end-diastolic volumes. These cycles all passed through the volume range near 20 ml, but did so early, late or in the middle of their ejections. Despite these differences in the history of the cardiac cycle the absolute strains were very similar in that volume range (volume strain ≈ -0.5).

When the absolute strains as a function of volume strain did not fall perfectly on a single common straight line, in addition to possible random measurement error, there could be either a systematic variation dependent

on preload and amount of ejection or a small deviation from the common line at the beginning or end of ejection. As an example of a systematic variation, in Fig. 6 the absolute strain E_{22} as a function of volume strain fell along four parallel lines, one per cardiac cycle. This was also true, for example, of the strain E_{11} of heart 3 in Fig. 8. These small differences in offset could be due to secondary effects of pressure and ejection history. However, the slopes were almost always identical. The small variation from linearity at the start of ejection (see strain E_{12} in Fig. 7) was probably due to the fact that the heart began to eject slightly before it had reached its preferred kinematic state.

We have also found that the kinematics of ejection was very different from the kinematics of filling (see Figs. 3, 4, and 5). This must be due to the contractile action of the sarcomeres that altered the effective material properties of the myocardium. This change in material response could not have been a uniform and isotropic stiffening that would only have increased the pressure generated at any given volume but not altered

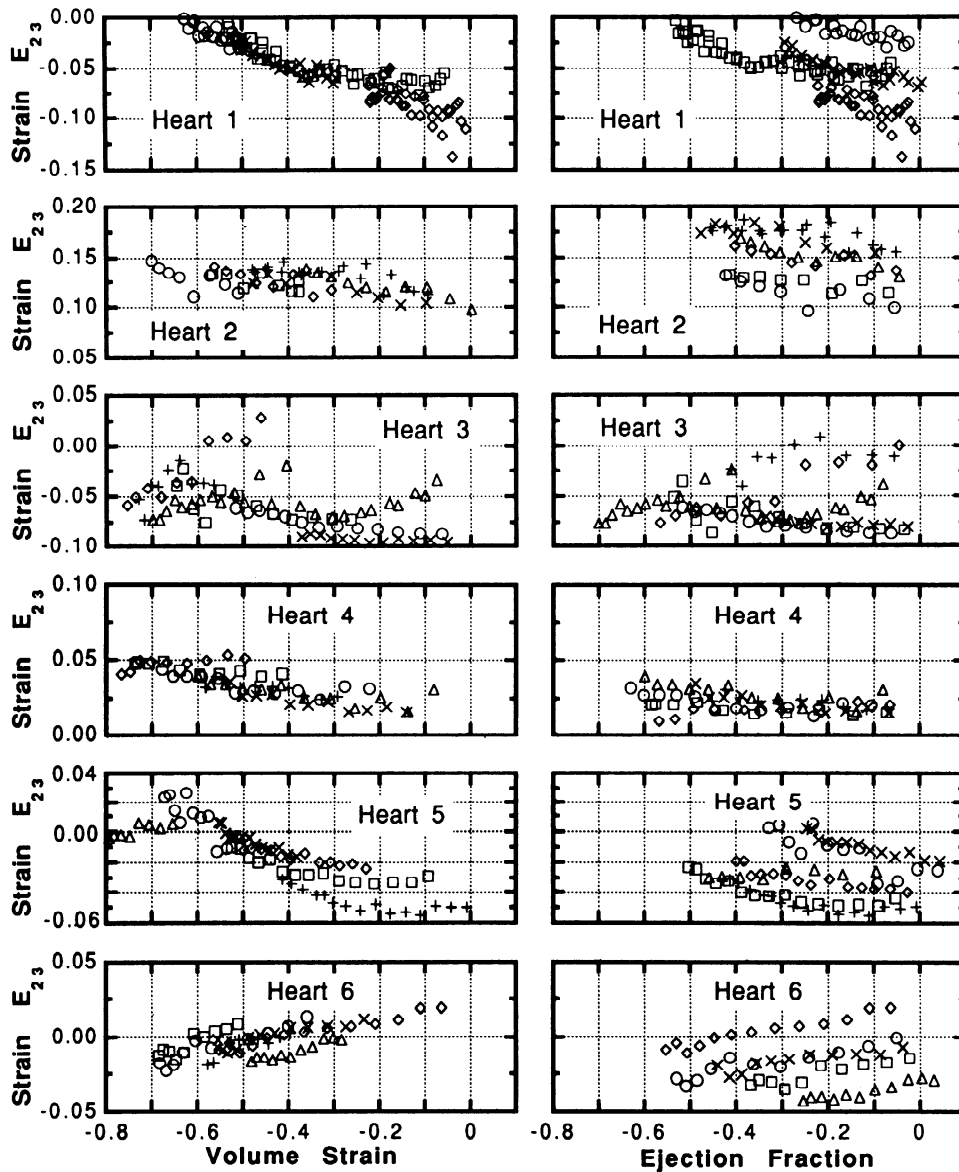


FIG. 10. Comparison among all 6 hearts of shear strain E_{23} as a function of volume strain and ejection fraction during ejection only. Note that the strain range for hearts 1-3 is 0.15, while the range for hearts 4-6 is 0.10.

the geometric configuration of the left ventricle. Instead, the transition from diastole to systole must have introduced a change in the degree of anisotropy (the relationship between stress and strain in different directions) and in the overall stiffness.

We have also observed that the strains, and hence, presumably, the sarcomere lengths, during ejection are largely independent of both the history of deformation and the ventricular pressure. Since the myocardium is a viscoelastic (time dependent) material, this observation was not necessarily expected. However, the apparent independence of sarcomere length on pressure and time may well be a result of a saturation effect. When the sarcomeres are fully contracting, they become much stiffer than passive myocardium (4). Thus the myocardial stiffness in the sarcomere direction becomes large relative to other directions, with the result that the shape of the left ventricle may be governed more by the relative stiffnesses in each direction rather than by the actual magnitude of stiffness in the direction of the sarcomeres. For example, a model based on total sarcomere domi-

nance of the myocardial mechanical behavior (1) follows similar fixed trajectories relating strain components during ejection. In fact, Fig. 3 in Ref. 1 shows how base-to-apex strain, circumferential strain, and shear angle are all uniquely related to volume strain independent of preload and afterload.

Finally, the unique relationship between strain and volume may allow a direct link to be built between muscle mechanics and ventricular mechanics. Simple models of the left ventricle have hypothesized that there is a unique relationship between sarcomere length and ventricular volume. Our results support the possibility that such a unique relationship might exist during ejection, independent of preload and afterload.

Comparison with other work on ventricular deformation. That the kinematics of the left ventricle are uniquely related to ventricular volume during ejection was also observed by Olsen et al. (17) by examining global changes in ventricular shape. By measuring ventricular eccentricity, Olsen et al. did not relate local structure to global function, but they did show that the

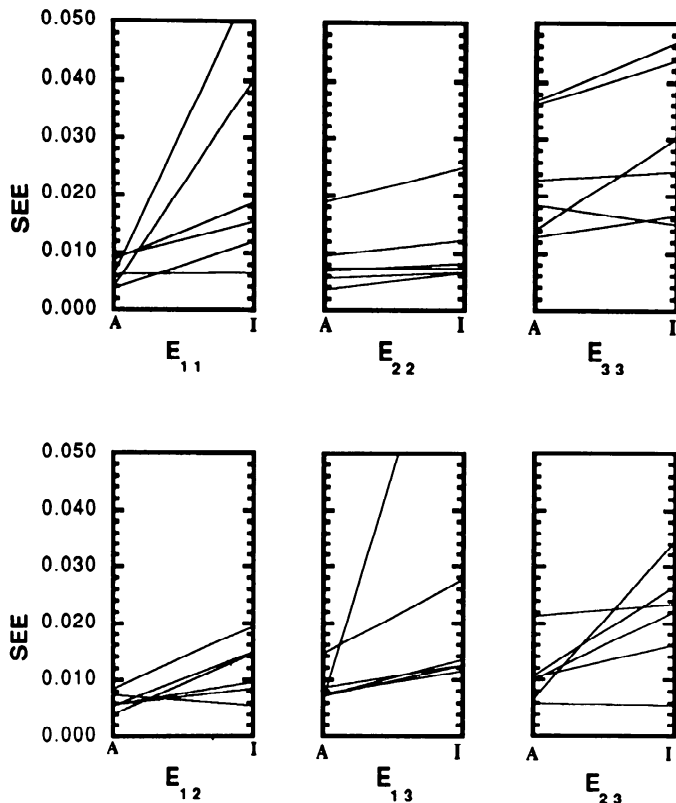


FIG. 11. Graphical representation of the difference between colinearity of absolute strain versus volume strain and individual strain vs. ejection fraction. Standard error of the estimate (SEE) derived from linear regression is plotted for absolute strains (A) and for individual strains (I). Each panel is one strain component. Each line represents change in SEE between absolute and individual strains.

shape (or kinematics) of the heart was different between ejection and filling and that, during ejection, the global shape of the heart was a unique function of volume. Their observations could not be explained as merely effects of ventricular pressure, because, while the ventricle was more spherical at large volume during diastole than during ejection, it was more elliptical at low volumes. Thus the complex local action of the sarcomeres gives rise to a different kinematics during diastole and ejection as pointed out above.

The change in the time course of two dimensional Lagrangian strains in the ventricular midwall with increasing EDP was reported by Villarreal et al. (25). As EDP increased, the change in the circumferential strain (E_{11} in Fig. 3 of Ref. 25) became dominant, indicating a strain history dependent on EDP. However, their strains were computed using the end-diastolic configuration as the reference state for each cycle (of increasing EDP). These strains can therefore be compared directly with the individual strain vs. ejection fraction plots shown in the right panels of Figs. 3 and 4. Their two-dimensional strains, reported as a function of time (Fig. 3 of Ref. 27), show that the strain range during ejection for E_{11} decreased with an increase in EDP while the strain range during ejection for E_{22} and E_{12} remained relatively constant. This is consistent with the behavior of the midwall individual strains E_{11} and E_{22} during ejection as shown here in the right panels of Fig. 3. Additionally, our data

(see also Fig. 8) are consistent with their observation that the principal shortening direction becomes more circumferential at larger EDP when referenced individually to the different end-diastolic configurations. However, when referenced to a single configuration the pattern of strain during ejection (including the principal strain direction) did not vary with preload.

In the isolated arrested heart, McCulloch et al. (13, 14) observed a linear relationship between stretch and volume by observing the two-dimensional straining of the epicardium. Although we have not systematically investigated filling, their observations are consistent with the relationship between the strains E_{11} and E_{22} and volume in *heart 1* (see Fig. 5) during passive filling found here.

While Waldman et al. (27, 28) were the first to examine three-dimensional strains in a local region of ventricular myocardium, they did not report on any changes in strain with preload and afterload. Regional differences in myocardial deformation were reported by Lew and LeWinter (11). The changes in normalized end-diastolic segment length as a function of EDP in the posterior region reported by Lew and LeWinter are consistent with the changes in the circumferential strains (E_{11}) shown in Fig. 3 when one examines P-V loops 1 and 3.

Although the isolated heart procedure used here introduces some changes in ventricular mechanics, it has several advantages. The first is that the introduction of the latex balloon allows accurate monitoring of the ventricular volume. The second is that the servo controller can simulate a wide range of hemodynamic conditions while precisely monitoring left ventricular pressure.

However, it is still important to mention the possible changes in strain that may result from the isolated heart preparation. The heart is removed from the pericardial sack and placed, horizontally, on a thin plastic membrane. This may tend to let gravity flatten the heart during diastole, changing the meridional and circumferential strains slightly. The mitral annulus is removed and a rigid mitral ring, which does not deform, is sutured into place, reducing the magnitude of all the strains near the mitral ring. The chordae tendinae are cut, which may alter the shear strain E_{23} . The right ventricle remains empty and does no work, which may affect strains in the septum and in a region of the left ventricular wall near the right ventricle. However, in the region of the ventricle for which strains are reported here, all these changes should be small. Finally, in the isolated heart the coronary perfusion pressure (CPP) remains constant despite changes in the systolic pressure generated by the left ventricle. While there have been suggestions that CPP can influence ventricular wall mechanics (26), the effect appears to be small in our preparation (22).

Role of reference state. Studies of local left ventricular deformation originated with observations of short segment lengths (24) via sonomicrometry. Because the purpose of these early studies was often to compare ischemic vs. normally perfused regions, the amount of active shortening during systole (as a percentage of end-diastolic length) was naturally chosen as the normalized measure to be examined. Since that time many studies of local

deformation (11, 25, 27, 28) have followed the convention of referencing systolic strains to the end-diastolic configuration in each beat. Others who have looked at global ventricle diameters have recommended the use of a single reference configuration (17, 18).

In this work, we used both a single reference configuration and one that varied with end-diastolic volume. If both the absolute strains and the volume strain were referenced to the single maximum-volume end-diastolic configuration, then there was a simpler picture of local deformation: all six strain components were uniquely and linearly related to volume strain during ejection. However, using the end-diastolic state for each beat, no consistent relationship between local deformation and ejected volume could be found.

The choice of the single reference state is arbitrary. Strains with reference to one configuration are directly related to the strains referenced to any other configuration (see APPENDIX B). Thus, if a unique relationship between absolute strain and volume strain exists for one choice of reference state, then a unique relation would exist for all choices of reference state. Indeed, a unique linear relationship between two-dimensional strain and volume strain was reported earlier (8, 9) when the strain and volume were referenced to an end-diastolic state at low volume (having zero transmural pressure), just as we report here using a maximal volume reference state.

Conclusion. We have thus established that, by using a single reference state, a unique relationship between strain and volume existed in the canine left ventricle independent of preload and afterload during ejection. On the other hand, the relationship between shortening fraction and ejection fraction was dependent on the history of cardiac deformation. This finding is consistent with the notion that active myocardium consistently assumes a preset cardiac configuration, dependent only on instantaneous ventricular volume and independent of the hemodynamic state.

APPENDIX A

Strain Computation

What follows is a brief but complete description of the method used to determine load ventricular strains from the recorded motion of six markers. The local cardiac coordinates are defined and the method of computing the deformation gradient is described.

Reference configurations. Because both the deformation gradient and strain are measured relative to some reference configuration, it is necessary to define this reference state unambiguously. While the reference state may be simple to define in most manufactured components because they, in general, possess an initial virgin stress-free state, this is not so in biological materials where stresses are present in almost all physiologically realizable configurations. All the strains presented here are measured relative to two reference configurations.

The first configuration is the end-diastolic state for the particular cardiac cycle in question. Since this is defined for only one cycle we called this configuration an "individual" reference state (i). In this state the six marker beads occupy the positions $\mathbf{X}_p^{(i)}$ ($p = 1, \dots, 6$). Each cardiac cycle has its own individual reference state.

The second reference state is the maximum volume end-diastolic state over all cardiac cycles observed for that heart. Since there is only one such reference state per heart we called this configuration an "absolute" reference state (a). In this reference state the six marker beads occupy the positions $\mathbf{X}_p^{(a)}$. There will always be one cardiac cycle, corresponding to the cycle which has the maximum end-diastolic volume, for which the two reference states coincide, viz. $\mathbf{X}_p^{(a)} = \mathbf{X}_p^{(i)}$.

Definition of deformation gradient tensor \mathbf{F} . The six radio-opaque marker beads at the vertices of a prism in the ventricular myocardium are defined by their respective positions \mathbf{X}_p in either of the end-diastolic reference states (individual or absolute) used, as measured with respect to the fixed laboratory coordinate system. During ejection the motion of the six radio-opaque marker beads was defined by the time history of their positions \mathbf{x}_p with respect to a fixed laboratory coordinate system. These positions were a function of the particular bead and of time; thus $\mathbf{x}_p = \mathbf{x}_p(\mathbf{X}_p, t)$. Note that, since at some time $t = t^{(i)}$, the markers occupy the end-diastolic (individual reference) state $\mathbf{x}_p(\mathbf{X}_p, t^{(i)}) = \mathbf{X}_p^{(i)}$ at time $t^{(i)}$.

The relative motion of any two neighboring points of material in the region spanned by the six marker beads was, in general, *inhomogeneous* (2). That is, the same relative motion was not common to all neighboring points within the region of the prism spanned by the six markers. With four marker beads that define a tetrahedron, only the *homogeneous* part of the motion could be determined. A full description of the three-dimensional inhomogeneous deformation in this region requires additional information (2), which includes the motion of additional beads to describe higher order gradients in displacement. Some of this information can be obtained from the extra two beads that define the prism. However, this additional information could also be used to obtain the optimal homogeneous deformation in the prism by minimizing errors in a least-squares manner (2).

Any relative motion could be broken down into a local relative rotation and a strain. The rigid-body translation of the two neighboring points caused no relative motion. Formally, if the two neighboring points had original relative position $d\mathbf{x}$ and relative position $d\mathbf{x}(t)$ at some time t later, then

$$d\mathbf{x}(t) = \mathbf{F}(t) \cdot d\mathbf{X} \quad (A1)$$

where \mathbf{F} is the deformation gradient tensor (12), which contained information about both local relative rotation and stretch.

If, as was assumed here, the deformation was homogeneous, then \mathbf{F} was constant in space and the motion of any general point, \mathbf{x} , in the region spanned by the prism with reference position \mathbf{X} , was given by integrating equation (2) to give

$$\mathbf{x}(\mathbf{X}, t) = \mathbf{F}(t) \cdot \mathbf{X} + \mathbf{b}(t) \quad (A2)$$

The deformation gradient tensor, $\mathbf{F}(t)$, here contained information about the local homogeneous rotation and stretching of myocardium in the prism region and $\mathbf{b}(t)$ was the rigid-body translation of the centroid of the prism from the reference configuration to its position at time t .

Cardiac coordinates. Since we were interested in local cardiac parameters, we wished to measure these parameters with respect to the heart. Thus it was necessary to introduce local cardiac coordinate axes, as common to all hearts investigated as possible, with which to examine local cardiac function. Two beads were used to define the longitudinal axis of the heart. The first was stitched to the apex of the heart, while the second was stitched as close to the long axis of the heart as possible in the basal region between the mitral and aortic valves near where the anterior leaflet of the mitral valve arises from the

mitral annulus. The location of the bead at the apex was given by \mathbf{X}_a , while that of the bead at the base was given by \mathbf{X}_b . The longitudinal axis of the heart in the reference configuration was then defined by the unit vector $\mathbf{l} = (\mathbf{X}_b - \mathbf{X}_a) / \|\mathbf{X}_b - \mathbf{X}_a\|$, represented by the line CD in Fig. 1.

The outward normal to the plane of the three beads on the epicardial surface in the reference configuration was given by the unit vector \mathbf{a}_3 (see Fig. 1), which defined the local radial direction. The local circumferential direction of the left ventricle was then in the direction of the unit vector $\mathbf{a}_1 = \mathbf{l} \times \mathbf{a}_3$. The local meridional direction (\mathbf{a}_2) is then given by $\mathbf{a}_2 = \mathbf{a}_3 \times \mathbf{a}_1$. Note that the orthonormal vectors \mathbf{a}_1 , \mathbf{a}_2 , and \mathbf{a}_3 remain fixed throughout a cardiac cycle.

Computation of deformation gradient. To compute the homogeneous deformation gradient \mathbf{F} within the region spanned by the six markers as a function of time, it was useful to redefine the marker positions in coordinates relative to the centroid using \mathbf{a}_1 , \mathbf{a}_2 , and \mathbf{a}_3 as unit base vectors. In the reference and deformed configurations respectively, the centroid was defined by

$$\bar{\mathbf{X}} = \sum_{p=1}^6 \mathbf{X}_p / 6 \quad \text{and} \quad \bar{\mathbf{x}} = \sum_{p=1}^6 \mathbf{x}_p / 6. \quad (A3)$$

Therefore, for each of the six marker beads ($p = 1-6$), the position relative to the centroid was given by

$$\mathbf{X}_p^* = \mathbf{X}_p - \bar{\mathbf{X}} \quad \text{and} \quad \mathbf{x}_p^*(t) = \mathbf{x}_p(t) - \bar{\mathbf{x}}(t). \quad (A4)$$

Substituting Eq. A4 into Eq. A2 gave the current positions of the markers relative to the current centroid in terms of the local deformation gradient and the reference positions of the markers relative to the centroid in that state, viz.

$$\mathbf{x}_p^*(t) = \mathbf{F}(t) \cdot \mathbf{X}_p^* \quad \text{for} \quad p = 1-6 \quad (A5)$$

If we define $[\mathbf{F}(t)]$ as the (3×3) matrix of components of the tensor $\mathbf{F}(t)$ and let the (3×6) matrices $[X^*]$ and $[x^*]$ be defined by

$$[X^*] = [\mathbf{X}_1^*, \mathbf{X}_2^*, \mathbf{X}_3^*, \dots, \mathbf{X}_6^*] \quad \text{and} \quad (A6a)$$

$$[x^*(t)] = [\mathbf{x}_1^*(t), \mathbf{x}_2^*(t), \mathbf{x}_3^*(t), \dots, \mathbf{x}_6^*(t)] \quad (A6b)$$

then, using the generalized inverse (16),

$$[\mathbf{F}(t)] = [x^*(t)][X^*]^T([X^*][X^*]^T)^{-1} \quad (A7)$$

Since the positions $[X^*]$ and $[x^*(t)]$ were given by the biplanar radiographic technique, the deformation gradient matrix, $[\mathbf{F}(t)]$, could be computed throughout the contractile motion of the heart.

Lagrangian strains. The Lagrangian strain tensor $\mathbf{E}(t)$ is defined (12) in terms of the deformation gradient \mathbf{F} , its transpose \mathbf{F}^T , and identity \mathbf{I} tensors, by

$$\mathbf{E}(t) = [\mathbf{F}^T(t) \cdot \mathbf{F}(t) - \mathbf{I}] / 2 \quad (A8)$$

which, at any particular time t , gives one-half of the change in squared length per unit reference squared length at time t . Thus, for arbitrary unit direction \mathbf{a} in the region of the six-marker prism, and axial strain in direction \mathbf{a} is

$$\left. \frac{(ds)^2 - (dS)^2}{2(dS)^2} \right|_{\mathbf{a}} = \mathbf{a} \cdot \mathbf{E} \cdot \mathbf{a} \quad (A9)$$

where dS is the reference length in direction \mathbf{a} and ds is the deformed length of that segment.

It should be noted that the strain is a measure of deformation that is independent of rigid body translation and rotation and that is zero for no deformation. If a region contracts in any

direction, the strain component in that direction is negative. Conversely, an elongation in a direction results in an associated positive strain component.

APPENDIX B

Changes in Strain with Reference State

For any deformable body the deformation gradient tensor \mathbf{F} maps points from one configuration to another. Consider three deformed states of a body: two fixed states X and Y and a time-varying state $Z(t)$. The mapping from state X to state Z is $\mathbf{F}(t)$, while the mapping from state Y to state Z is $\mathbf{F}_2(t)$. The strains in state Z using state X as a reference are given by $2\mathbf{E}^{(X)} = \mathbf{F}^T \cdot \mathbf{F} - \mathbf{I}$, and the strains in state Z using state Y as a reference are given by $2\mathbf{E}^{(Y)} = \mathbf{F}_2^T \cdot \mathbf{F}_2 - \mathbf{I}$. Since we can arrive at state Z from state X via state Y , $\mathbf{F}(t) = \mathbf{F}_2(t) \cdot \mathbf{F}_1$, where \mathbf{F}_1 is the constant mapping from state X to state Y . The relationship between $\mathbf{E}^{(X)}$ and $\mathbf{E}^{(Y)}$ is then given by

$$2\mathbf{E}^{(X)} = \mathbf{F}_1^T \cdot \mathbf{F}_2^T \cdot \mathbf{F}_2 \cdot \mathbf{F}_1 - \mathbf{F}_1^T \cdot \mathbf{F}_1 + \mathbf{F}_1^T \cdot \mathbf{F}_1 - \mathbf{I} \quad (B1)$$

$$= 2\mathbf{F}_1^T \cdot \mathbf{E}^{(Y)} \cdot \mathbf{F}_1 + \mathbf{F}_1^T \cdot \mathbf{F}_1 - \mathbf{I} \quad (B2)$$

Because \mathbf{F}_1 is constant, if $\mathbf{E}^{(Y)}$ is a function of some time varying parameters, so is $\mathbf{E}^{(X)}$. Thus, if the strain in one fixed reference state is a function of, for example, volume, then the strain in any other fixed reference state is also a function of volume. The relationship between $\mathbf{E}^{(X)}$ and $\mathbf{E}^{(Y)}$ is, in general, complex. However, if the rotation \mathbf{R}_1 is small ($\mathbf{F}_1 = \mathbf{R}_1 \cdot \mathbf{U}_1$, where \mathbf{U} is the stretch tensor), then the relationship between the principal strains of $\mathbf{E}^{(X)}$ and the principal strains of $\mathbf{E}^{(Y)}$ is linear.

The authors thank Dr. James H. Anderson, Michael Samphilipo, Carolyn Magee and Frank L. Starr for their assistance with the biplane cineradiographic procedures. We also appreciate the help of Dr. Willard Graves and David Mearns for assistance with the marker tracking software. Sincere thanks also go to Ken Rent, who provided invaluable surgical assistance, to Yuske Sagawa and Peter Komarow, who spent many hours tracking markers on film, and to Jeffrey W. Holmes and Michelle J. Royce for their help in the computations.

This work was supported by National Heart, Lung, and Blood Institute Grant HL-30552. W. C. Hunter was the recipient of Research Career Development Award K04-HL-01232.

Present address of E. K. Rodriguez: Dept. of Applied Mechanics and Engineering Science, University of California, San Diego, La Jolla, CA 92093-0413.

Address for reprint requests: A. S. Douglas, Dept. of Mechanical Engineering, 127 Latrobe Hall, Johns Hopkins University, Baltimore, MD 21218.

Received 11 July 1990; accepted in final form 10 December 1990.

REFERENCES

- ARTS, T., P. C. VEENSTRA, AND R. S. RENEMAN. Epicardial deformation and left ventricular wall mechanics during ejection in the dog. *Am. J. Physiol.* 243 (*Heart Circ. Physiol.* 12): H379-H390, 1982.
- DOUGLAS, A. S., W. C. HUNTER, AND M. D. WISEMAN. Inhomogeneous deformation as a source of error in strain measurement derived from implanted markers in the canine left ventricle. *J. Biomech.* 23: 331-341, 1990.
- FENTON, T. R., J. M. CHERRY, AND G. A. KLASSEN. Transmural myocardial deformation in the canine left ventricular wall. *Am. J. Physiol.* 225: H523-H530, 1978.
- FUNG, Y. C. *Biomechanics*. New York: Springer-Verlag, 1981.
- GARRISON, J. B., W. L. ELBERT, R. E. JENKINS, S. M. YIONOULIS, H. MALCOM, G. A. HELLER, A. A. SHOUKAS, W. L. MAUGHAN, AND K. SAGAWA. Measurement of three-dimensional positions and motions of large numbers of spherical radiopaque markers from

- biplane cineradiograms. *Comput. Biomed. Res.* 15: 76–96, 1982.
6. GLANTZ, S. A., AND B. K. SLINKER. *Primer of Applied Regression and Analysis of Variance*. New York: McGraw-Hill, 1990, p. 16–24.
 7. HITTINGER, L., B. CROZATIER, J.-P. BELOT, AND M. PIERROT. Regional ventricular segmental dynamics in normal conscious dogs. *Am. J. Physiol.* 253 (*Heart Circ. Physiol.* 22): H713–H719, 1987.
 8. HUNTER, W. C., A. S. DOUGLAS, E. K. RODRIGUEZ, AND J. W. HOLMES. Local versus global deformation in left ventricles of isolated hearts (Abstract). *ASME Applied Mech. Eng. Sci. Conf. Berkeley 1988*, p. 87.
 9. HUNTER, W. C., A. S. DOUGLAS, Y. SAGAWA, J. W. HOLMES, AND E. K. RODRIGUEZ. Local strains in LV myocardium: uniquely determined by volume during ejection? (Abstract). *Circulation* 80: II-224, 1988.
 10. HUNTER, W. C., AND E. A. ZERHOUNI. Imaging distinct points in left ventricular myocardium to study regional wall deformation. In: *Innovations in Diagnostic Radiology*, edited by J. H. Anderson. New York: Springer-Verlag, 1989, 169–190.
 11. LEW, W. Y. W., AND M. M. LEWINTER. Regional comparison of midwall segment and area shortening in the canine left ventricle. *Circ. Res.* 58: 678–691, 1986.
 12. MALVERN, L. E. *Introduction to the Mechanics of a Continuous Medium*. Englewood Cliffs, NJ: Prentice-Hall, 1969.
 13. MCCULLOCH, A. D., B. H. SMAIL, AND P. J. HUNTER. Left ventricular epicardial deformation in isolated arrested dog heart. *Am. J. Physiol.* 252 (*Heart Circ. Physiol.* 21): H233–H241, 1987.
 14. MCCULLOCH, A. D., B. H. SMAIL, AND P. J. HUNTER. Regional left ventricular epicardial deformation in the passive dog heart. *Circ. Res.* 64: 721–733, 1989.
 15. MEIER, G. D., M. C. ZISKIN, W. P. SANTAMORE, AND A. A. BOVE. Kinematics of the beating heart. *IEEE Trans. Biomed. Eng.* 27: 319–329, 1980.
 16. NOBLE, B. *Applied Linear Algebra*. Englewood Cliffs, NJ: Prentice-Hall, 1969.
 17. OLSEN, C. O., J. S. RANKIN, C. E. ARENTZEN, W. S. RING, P. A. MCHALE, AND R. W. ANDERSON. The deformation characteristics on the left ventricle in the conscious dog. *Circ. Res.* 49: 843–855, 1981.
 18. RANKIN, J. S., C. E. ARENTZEN, P. A. MCHALE, D. LING, AND R. W. ANDERSON. Viscoelastic properties of the diastolic left ventricle in the conscious dog. *Circ. Res.* 41: 37–45, 1977.
 19. SHOUKAS, A. A., K. SAGAWA, AND W. L. MAUGHAN. Chronic implantation of radiopaque beads on endocardium, midwall, and epicardium. *Am. J. Physiol.* 241 (*Heart Circ. Physiol.* 10): H104–H107, 1981.
 20. STREETER, D. D., JR. Gross morphology and fiber geometry of the heart. In: *Handbook of Physiology. The Cardiovascular System. The Heart*. Bethesda, MD: Am. Physiol. Soc., 1979, sect. 2, vol. 1, chapt. 4, p. 61–112.
 21. SUGA, H., AND K. SAGAWA. End-diastolic and end-systolic ventricular volume clamped for isolated canine heart. *Am. J. Physiol.* 233 (*Heart Circ. Physiol.* 2): H718–H722, 1977.
 22. SUGIURA, S., W. C. HUNTER, M. A. WACLAWIWI, AND K. SAGAWA. Dynamic properties of left ventricular response to changes in coronary perfusion. *Am. J. Physiol.* 260 (*Heart Circ. Physiol.* 29): H1332–H1343, 1991.
 23. SUNAGAWA, K., D. BURKHOFF, K. O. LIM, AND K. SAGAWA. Impedance loading servo pump system for excised canine ventricle. *Am. J. Physiol.* 243 (*Heart Circ. Physiol.* 12): H346–H350, 1982.
 24. THEROUX, P., D. FRANKLIN, J. ROSS, JR., AND W. S. KEMPER. Regional myocardial function during acute coronary occlusion and its modification by pharmacologic agents. *Circ. Res.* 35: 896–908, 1974.
 25. VILLARREAL, F. J., L. K. WALDMAN, AND W. Y. W. LEW. Technique for measuring regional two-dimensional finite strains in canine left ventricle. *Circ. Res.* 62: 711–721, 1988.
 26. VOGEL, W. M., C. S. APSTEIN, L. L. BRIGGS, W. H. GAASCH, AND J. AHN. Acute alterations in left ventricular diastolic chamber stiffness: role of the “erectile” effect of coronary arterial pressure and flow in normal and damaged hearts. *Circ. Res.* 51: 465–478, 1982.
 27. WALDMAN, L. K., Y. C. FUNG, AND J. W. COVELL. Transmural myocardial deformation in the canine left ventricle. Normal in vivo three-dimensional finite strains. *Circ. Res.* 57: 152–163, 1985.
 28. WALDMAN, L. K., D. NOSAN, F. VILLARREAL, AND J. W. COVELL. Relation between transmural deformation and local myofiber direction in canine left ventricle. *Circ. Res.* 63: 550–562, 1988.